Volume 12
Number 36
28 September 2024
Pages 8803–9100

Journal of Materials Chemistry B

Materials for biology and medicine

rsc.li/materials-b

ISSN 2050-750X

ROYAL SOCIETY OF CHEMISTRY

PAPER

Yang Wang, Chenggang Duan, Zuoying Yuan *et al.*
High-purity butoxydibutylborane catalysts enable the low-exothermic polymerization of PMMA bone cement with enhanced biocompatibility and osseointegration

Journal of Materials Chemistry B

PAPER

Published on 06 August 2024
Licence and permissions

Check for updates

Cite this: J. Mater. Chem. B, 2024, 12, 8911

High-purity butoxydibutylborane catalysts enable the low-exothermic polymerization of PMMA bone cement with enhanced biocompatibility and osseointegration†

Zhuo Wan,‡[a] Yike Gao,‡[b] Yingbo Wang,‡[c] Xianghao Zhang,[c] Xiyin Gao,[d] Tuanfeng Zhou,[c] Zhishan Zhang,[e] Zijian Li,[e] Yunfei Lin,[f] Bing Wang,[f] Kun Chen,[a] Yang Wang,*[c] Chenggang Duan*[c] and Zuoying Yuan *[ag]

Polymethyl methacrylate (PMMA) based biomaterials have been widely utilized in clinics. However, currently, PMMA catalyzed by benzoyl peroxide (BPO) exhibits disquieting disadvantages including an exothermic polymerization reaction and a lack of bioactivity. Here, we first designed three industrial-scale synthesis methods for high-purity butoxydibutylborane (BODBB), achieving purity levels greater than 95% (maximum: 97.6%) and ensuring excellent fire safety. By utilizing BODBB as a catalyst, the highest polymerization temperature of PMMA bone cement (PMMA–BODBB) reached only 36.05 °C, ensuring that no thermal damage occurred after implantation. Compared to PMMA catalyzed by BPO and partially oxidized tributylborane (TBBO, catalyst of Super Bond C&B), PMMA–BODBB exhibited superior cell adhesion, proliferation, and osteogenesis, attributed to the reduced release of free radicals and toxic monomer, and moderate bioactive boron release. After injection into a 5 mm defect in the rat cranial bone, PMMA–BODBB demonstrated the highest level of osteointegration. This work not only presents an industrial-scale synthesis of high-purity BODBB, but also offers an innovative PMMA biomaterial system with intrinsic biocompatibility and osseointegration, paving the way for the next generation of PMMA-based biomaterials with broader applications.

Received 6th May 2024,
Accepted 4th August 2024

DOI: 10.1039/d4tb00967c

rsc.li/materials-b

Introduction

For over 70 years, polymethyl methacrylate (PMMA) based biomaterials have been extensively used in various clinical applications, including fracture fixation, cone shaping procedures, bone defect filling, bone tumor treatment, dental prosthesis repair, contact lenses, and medical aesthetic fillers.[1–4] In orthopedic clinics, PMMA stands out as the most extensively applied polymer-based bone cement due to its excellent mechanical properties, shape adaptability, and chemical stability.[5,6] Nonetheless, prolonged clinical use has revealed detrimental effects of PMMA on tissue regeneration, such as inadequate bone integration and inhibition of new bone growth due to its biologically inactive nature, thermal damage to surrounding tissues caused by high temperatures during polymerization, and cytotoxicity resulting from incomplete polymerization of MMA monomers.[7–10]

In recent years, researchers worldwide have dedicated efforts to modify PMMA bone cement to address these concerns.[11] The most extensively studied approach revolves around the integration of bioactive fillers, such as hydroxyapatite,[12] mineralized collagen,[13] nanoclay,[14] carbon nanomaterials,[15] and bioactive

[a] Department of Mechanics and Engineering Science, College of Engineering, Peking University, Beijing 100871, P. R. China
[b] Laboratory of Tissue Regeneration and Immunology and Department of Periodontics, Beijing Key Laboratory of Tooth Regeneration and Function Reconstruction, School of Stomatology, Capital Medical University, Beijing 100050, P. R. China
[c] Department of Oral and Maxillofacial Surgery, The First Clinical Division, The Third Clinical Division, and The Fifth Clinical Division, Peking University School of Stomatology, 100020 Beijing, P. R. China. E-mail: wyly78@sina.com, chenggang93@sina.com
[d] Key Laboratory of Science and Technology on High-tech Polymer Materials, Institute of Chemistry, Chinese Academy of Sciences, Beijing 100190, P. R. China
[e] Department of Orthopedics, Peking University Third Hospital, Beijing 100191, P. R. China
[f] Department of Orthopaedic Surgery, Peking University First Hospital, Beijing 100034, P. R. China
[g] Department of Biomedical Engineering, College of Future Technology, Peking University, Beijing 100871, P. R. China. E-mail: zy_yuan@pku.edu.cn

† Electronic supplementary information (ESI) available. See DOI: https://doi.org/10.1039/d4tb00967c

‡ These authors contribute equally.

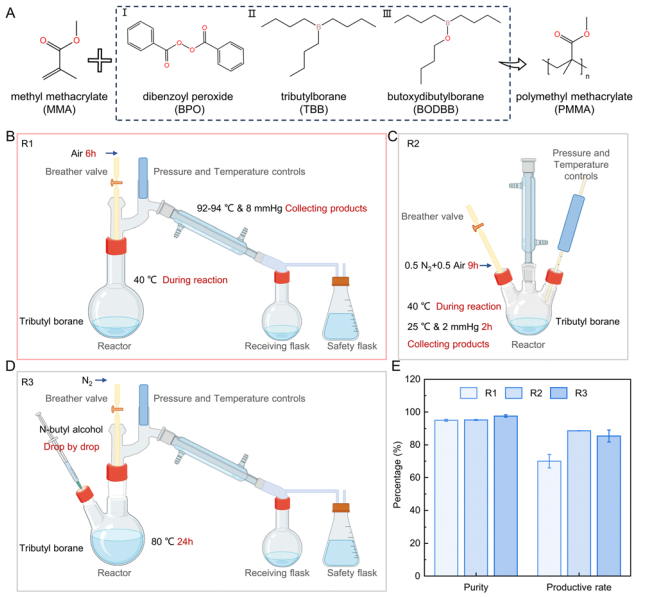

Fig. 1 (A) BPO-, TBB-, and BODBB-based catalytic systems for the polymerization of PMMA. Schematic diagram of the synthesis of high-purity BODBB *via* (B) air oxidation followed by fractional distillation, (C) nitrogen/air mixed gas oxidation, and (D) reaction of TBB with *n*-butanol followed by fractional distillation. (E) The productive rate and the purity of BODBB synthesized through various routes.

glass,[16] into PMMA to mitigate polymerization heat and enhance bone integration. Specifically, the inclusion of degradable biomaterials can generate porous structures in PMMA through the degradation of the dispersed phase, creating room for host cell infiltration and new bone formation.[17,18]

Enhancing biocompatibility and safety is the primary goal of PMMA bone cement modification.[11] However, many studies have failed to achieve significant improvements due to the inherent characteristics of the PMMA-initiating system, specifically, the benzoyl peroxide (BPO) catalyzed MMA polymerization (Fig. 1A, I).[19,20] To replace the BPO-based catalytic system, Masuhara developed a partially oxidized form of tributylborane (TBB) (Fig. 1A, II), known as TBBO, to initiate MMA-based resin for dental use in 1978.[21] The TBBO–MMA based resin, and its modified version, containing 4-META, called MMA-TBB/4-META resin (*i.e.*, Super-Bond C&B) was widely used and found to have a very good biocompatibility.[22] Hamajima investigated the use of TBBO as an initiator, which significantly reduced PMMA cytotoxicity and facilitated bone conduction by reducing the levels of free radicals at the interfaces.[23,24] Nevertheless, since this TBBO, as reported is a mixture containing 75% butoxydibutylborane (BODBB) (Fig. 1A, III),[25] still retains some flammability, and necessitates the use of additional hydrocarbon during the practical application, which harms the health of individuals. Therefore, there is an urgent need to synthesize high-purity BODBB with excellent storage safety as a catalyst to achieve low-temperature polymerization of PMMA bone cement with exceptional biocompatibility and osteointegration.

In this work, we first designed three industrial-scale synthesis methods for high-purity butoxydibutylborane (BODBB), achieving purity levels greater than 95% (maximum: 97.6%) and ensuring excellent fire safety. By utilizing BODBB as a catalyst, PMMA bone cement (PMMA–BODBB) with exceptional biocompatibility and osteointegration properties was obtained. During polymerization, the highest temperature reached only 36.05 °C according to ISO 5833, ensuring that no thermal damage occurred after implantation. Compared to PMMA catalyzed by BPO (PMMA–BPO) and PMMA catalyzed by partially oxidized tributylborane (TBBO, catalyst of Super Bond C&B) (PMMA–TBBO), PMMA–BODBB exhibited comparable mechanical properties, as well as superior cell adhesion, proliferation, and osteogenesis, attributed to the reduced release of free radicals and toxic monomer, and moderate bioactive boron release. After injection into a 5 mm defect in the rat cranial bone, PMMA–BODBB demonstrated the highest level of osteointegration, with the new bone volume fraction (BV/TV) and bone mineral density (BMD) reaching 33.33% and 129.36 mg cm^{-3}, respectively. This work not only presents an industrial-scale synthesis of high-purity BODBB, but also offers an innovative PMMA biomaterial system with intrinsic biocompatibility and osseointegration, paving the way for the next generation of PMMA-based biomaterials with broader applications.

Experimental

Materials

Polymethyl methacrylate (PMMA) powder, methyl methacrylate (MMA), and tributylborane (TBB) were procured from Guangdong Zhongkang Yingfei Biotechnology Co., Ltd (China). Benzoyl peroxide (BPO) was sourced from Heraeus (Germany). Additionally, partially oxidized tributylborane (TBBO) was acquired from Super Bond C&B (Japan). All other reagents and solvents utilized in our experiments were analytical grade and supplied by Beijing Chemical Reagent Co., Ltd (China).

Synthesis of high-purity butoxydibutylborane (BODBB)

To achieve high-purity BODBB on an industrial scale, three technological routes were formulated. In the first route, the reactor operated in a nitrogen environment with 1 mole of TBB introduced. The reaction temperature was controlled to remain below 40 °C, and dry air was incrementally introduced into the liquid surface of the reaction mixture while stirring continuously. Within 6 to 9 hours, an air volume corresponding to 0.5 moles of oxygen was added, inducing the partial oxidation of TBB. The partially oxidized TBB was then subjected to vacuum distillation under nitrogen, resulting in a fraction distilling at 92–94 °C/8 mmHg, thereby isolating the target BODBB.

In Route 2, conducted under a nitrogen atmosphere, 1 mole of tributylborane (TBB) was introduced into the reactor. The reaction temperature was meticulously controlled below 40 °C using a water bath. Dry nitrogen and air were incrementally introduced into the liquid TBB under constant stirring. Following this, the reaction vessel was exposed to reduced pressure (1–2 mmHg) at ambient temperature for 2 hours to yield the

This journal is © The Royal Society of Chemistry 2024

target product. The production rate and purity of BODBB were meticulously controlled by adjusting the nitrogen-to-air volume ratio (ranging from 0.5 : 1 to 2 : 1), the oxygen supply flow rate (between 0.43 and 0.86 L h^{-1}), and the duration of the gas mixture supply (spanning 6–12 hours).

In Route 3, the procedure was analogous to the previous routes, with the introduction of 1 mole of tributylborane (TBB) into the reactor under a nitrogen atmosphere. The reaction temperature was carefully controlled below 80 °C with continuous stirring, during which anhydrous *n*-butanol was added dropwise in a gradual manner. The mixture was then continuously heated to achieve a near-circulating flow status. After a 24-hour reaction period, heating was discontinued, resulting in the yield of the target bis(2-oxo-3-butyl)borane (BODBB). The synthesized BODBB was characterized using boron-11 (B11) and carbon-13 (C13) nuclear magnetic resonance (NMR) spectroscopy, with instrumentation provided by Bruker, Germany.

Preparation of polymethyl methacrylate (PMMA)

Polymethyl methacrylate initiated with BPO (PMMA–BPO) and with TBBO (PMMA–TBBO) were prepared following the manufacturer's instructions. For the preparation of PMMA–BODBB, the liquid MMA monomer and liquid BODBB were combined with the pre-polymerized PMMA powder to initiate the polymerization. This process was conducted at room temperature (23 °C) for a duration of 20 minutes subsequent to thorough mixing of the powder.

Characterization of polymethyl methacrylate (PMMA)

The polymerization reaction was monitored at temperatures of 23 °C and 37 °C, under conditions of 50% relative humidity. A 20-milliliter syringe barrel was utilized as the reaction vessel for the polymerization of methyl methacrylate (MMA). The temperature fluctuations throughout the polymerization process were meticulously assessed.

The thermal transitions of the end products, PMMA–TBBO and PMMA–BODBB, were investigated using differential scanning calorimetry (DSC) with a TA Q2000 instrument. Initially, the samples were subjected to a heating protocol to 150 °C to erase their prior thermal history, followed by rapid cooling to 0 °C at a rate of 60 °C per minute. Subsequently, the samples were reheated at a rate of 10 °C per minute up to a final temperature of 200 °C. Gel permeation chromatography (GPC) was used for analyzing *via* an Agilent PL-GPC 50, calibrated with a conventional calibration curve using monodisperse PMMA standards. Tetrahydrofuran (THF) was used as a carrier solvent at the flow rate of 0.10 mg mL^{-1}. Fourier transform infrared (FT-IR) spectra were obtained on a Thermo Fisher Scientific Nicolet iS20. The morphology of bone cements was examined using a scanning electron microscope (SEM, JEOL JSM-7500F, Japan).

Subsequently, the polymerized PMMA–BPO, PMMA–TBBO, and PMMA–BODDB were immersed in a phosphate-buffered saline (PBS) solution (pH = 7.4) at a mass-to-volume ratio of 0.1 g mL^{-1}. These solutions were agitated in a thermostatic water bath (60 rpm, 37 ± 1 °C). Extracted liquids were collected after 1 and 5 days, and the release of MMA monomer was analyzed using a spectrophotometer (NanoDrop 2000, Thermo Scientific). Additionally, the extract liquids were refreshed with PBS after 1, 3, 7, 14, and 21 days, and the concentration of released boron at each time point was measured using inductively coupled plasma optical emission spectrometry (ICP, PerkinElmer, Optima 7000DV, USA).

Compression tests were conducted using an STS10 N tensometer (Xiamen East Instrument Co. Ltd) equipped with a 1000 N load cell at a crosshead speed of 10 mm min^{-1}. Following ISO 5833:2002 guidelines, a polytetrafluoroethylene mold was employed to fabricate cylinders with a diameter of 6 mm and a thickness of 12 mm for compression testing.

Bovine sclerites were utilized to evaluate the lap shear strength. These sclerites were sectioned into rectangular bars measuring 1 × 4 × 0.5 cm and bonded with a 0.5 mm overlap using bone cement prepolymer. The specimens were secured in a shear bond strength apparatus, which was integrated with a universal testing machine. The peak force exerted during the test was recorded in Newtons (N) on a computer, and subsequently, this value was divided by the area of the bonded interface, expressed in square millimeters (mm^2), to ascertain the bond strength in Megapascals (MPa).

In vitro biosafety and osteoconductive capacity of the PMMA–BODBB bone cement

Sprague–Dawley (SD) rat BMSCs were purchased from Cyagen Biosciences (Guangzhou, China). The tested bone cements were immersed in complete medium or osteoinductive medium to make extracts, or osteoinductive extracts, and sterilized with a 0.2 μm filter. The detailed procedures for the tests of *in vitro* biosafety and osteoconductive capacity of the PMMA–BODBB bone cement are provided in the ESI.†

Rat calvarial defect model

All the animal experiments were complied with the guidelines of the Tianjin Medical Experimental Animal Care, and animal protocols were approved by the Institutional Animal Care and Use Committee of Yi Shengyuan Gene Technology (Tianjin) Co., Ltd (protocol number YSY-DWLL-2024307). Twelve female SD rats (5–6 weeks old) were utilized to induce a 5 mm calvarial defect for *in vivo* study. The defects were randomly allocated into 4 groups (10 rats per group) and treated as follows: (1) the control group, with the defect left unfilled; (2) the BPO group, with the defect filled with PMMA–BPO; (3) the TBBO group, with the defect filled with PMMA–TBBO; and (4) the BODBB group, with the defect filled with PMMA–BODBB. The detailed procedures for animal experiments are provided in the ESI.†

Statistical analysis

All quantitative data were expressed as mean ± standard deviation (SD) for $n \geq 3$. Statistical analysis was carried out using one-way analysis of variance (ANOVA) using Tukey's test. Differences between groups of $^*p < 0.05$ were considered

statistically significant, $^{**}p < 0.01$, $^{***}p < 0.001$, and $^{****}p < 0.0001$ was considered highly significant.

Results and discussion

The synthesis of the PMMA polymerization initiator system

In order to produce high-purity BODBB on an industrial scale, three technological routes have been designed. In Route 1, (Fig. 1B) the partial oxidation of TBB with a productive rate of 89.6%, and the content of BODBB in the partially oxidized TBB was 82.2% (Fig. S1, ESI†) The partially oxidized TBB was then subjected to vacuum distillation under a nitrogen environment. A fraction at 92–94 °C/8 mmHg was collected, leading to the isolation of the target BODBB with a productive rate of 70 ± 4.1%, and the purity was 95.0 ± 0.6%. In Route 2, (Fig. 1C) the productive rate and purity of BODBB could be controlled by adjusting the volume ratio of nitrogen/air, oxygen supply flow rate, and supply duration of the gas mixture. (Fig. S2–S5, ESI†) When the volume ratio of nitrogen/air was 1 : 1, the oxygen supply flow rate was 0.57 L h^{-1}, and the supply duration was 9 hours, the productive rate of BODBB was 88.6 ± 0.1%, while the purity was 95.2 ± 0.3%. In Route 3, (Fig. 1D) similarly, 1 mol of TBB was injected into the reactor under a nitrogen environment. The reaction temperature was maintained below 80 °C under stirring, and 1 mol of anhydrous *n*-butanol was gradually added dropwise. The mixture was then continuously heated to achieve the near-circulating flow status. After 24 hours of reaction, the heating was stopped, and the target BODDB was obtained with a productive rate of 85.4 ± 3.7%, while the purity was 97.6 ± 0.8%.

The representative B11 and C13 nuclear magnetic resonance (NMR) spectrum is shown in Fig. S6 (ESI†). Regardless of the employed technological route, BODBB with a high purity of over 95% was achieved. Additionally, upon dropping 0.5 mL of obtained BODBB onto filter paper maintained at 23 °C ± 2 °C, no hints of smoking, charring, or ignition were observed, indicating its excellent fire safety. Among these three routes, the productive rate of Route 1 was too low for economic industrial production. Route 2 had a simple production process and a relatively high productive rate, while Route 3 achieved the highest purity of BODBB, reaching 97.6%. Hence, subsequent experiments utilized BODBB synthesized *via* Route 3. (Fig. 1E).

Preparation and characterization of the PMMA–BODBB bone cement

To verify the clinical feasibility of BODBB, we explored its usage by mimicking the operation process of Super Bond C&B. By mixing with MMA monomers and PMMA powder, the prepolymer of PMMA–BODBB can undergo easy perfusion or smearing in the affected area (Fig. 2A) Its injectability was also demonstrated in the presentation of Fig. 2B. To verify the performance of PMMA–BODBB, the commercially available PMMA bone cement initiated by BPO was used as a control, we tested their exothermic levels at 23 °C and 37 °C (Fig. 2C). First, the ambient temperature was set to 23 °C. Compared with

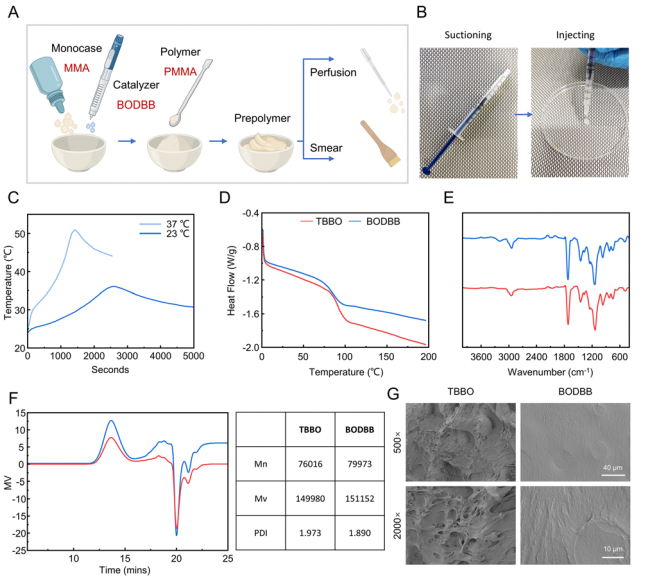

Fig. 2 (A) The potential operation method of PMMA–BODBB in the clinic. (B) The injectability of PMMA–BDDOB. (C) Temperature changes in the process of polymerization using BODDB as a catalyst. DSC. (D) Differential scanning calorimetry (DSC), (E) Fourier transform infrared (FTIR) spectroscopy, (F) gel permeation chromatography (GPC), and (G) SEM images of PMMA–TBBO and PMMA–BODBB.

the highly exothermic PMMA–BPO (Fig. S7. ESI†), the polymerization temperature of PMMA–BODBB was only 36.05 °C. At an ambient temperature of 37 °C, which simulates the human body, the polymerization temperature of PMMA–BPO reached over 87.15 °C, while PMMA–BODBB exhibited significantly lower exothermic peaks at only 50.96 °C.

Subsequently, we verified the polymerization performance of the final PMMA product by using Super Bond C&B as a control. DSC showed that both PMMA–BODBB and PMMA–TBBO exhibited similar glass transition states in the 75–100 °C range (Fig. 2D), and the infrared spectra also similarly displayed identical functional groups (Fig. 2E). GPC results indicated that PMMA–BODBB has a higher molecular weight and a more concentrated polydispersity index (PDI) compared to PMMA–TBB (Fig. 2F). These results prove that BODBB, as a bone cement polymerization catalyst has achieved efficient and low exothermic production, which is critical for avoiding thermal damage to tissues caused by cement implantation, and its final product is similar to commercial products (Super Bond C&B).

Mechanical properties of the PMMA–BODBB bone cement

The PMMA–BODBB exhibits comparable mechanical properties to PMMA–TBBO (Fig. 3A) with a compressive strength of 100.33 MPa (Fig. 3B) and a Young's modulus of 2517.20 MPa (Fig. 3C), ensuring the mechanical stability of PMMA–BODBB after implantation. The bonding strength of PMMA–TBBO and PMMA–BODBB to bone tissue reached approximately 1.03 MPa and 0.96 MPa at 10 minutes. After 1 hour, the bonding strength of PMMA–TBBO and PMMA–BODBB increased to 1.38 MPa and 1.45 MPa attributed to the complete polymerization (Fig. 3D).

This journal is © The Royal Society of Chemistry 2024

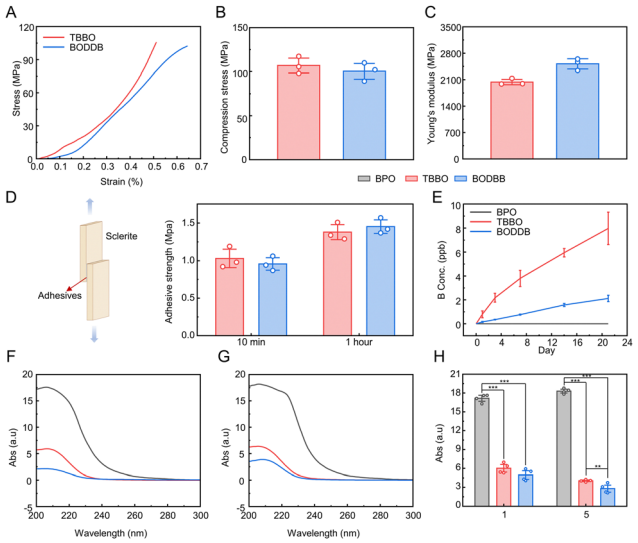

Fig. 3 (A) Compressive curves, (B) compressive strength and (C) Young's modulus of PMMA–TBBO and PMMA–BODDB. (D) Lap shear strength of PMMA–TBBO and PMMA–BODDB with Sclerites after adhesion. (E) Cumulative release concentrations of boron from various PMMA within the experimental period of 21 days in PBS at 37 °C. The ultraviolet spectrogram of released MMA monomer for (F) 1 day and (G) 5 days. (H) The release of MMA monomer from various PMMA.

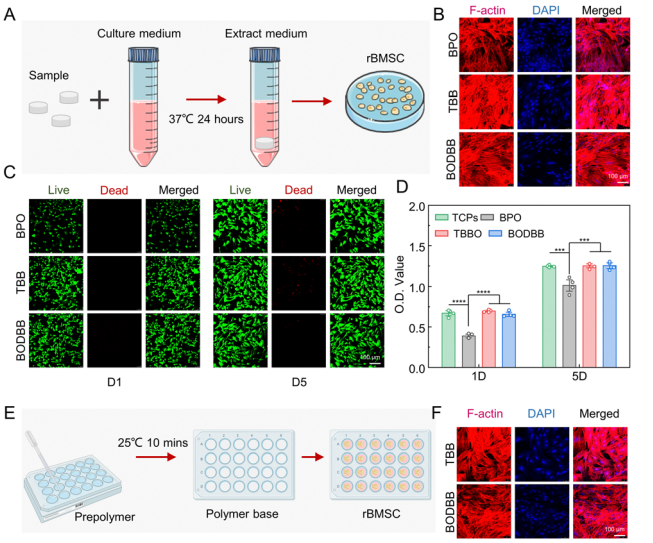

Fig. 4 (A) Schematic diagram of the preparation of extracts, rBMSCs were cultured with extracts. (B) Cell morphology was captured after Phalloidin–Hoechst staining on day 5. (C) The viability of rBMSCs was observed by live/dead staining on Day 1 and Day 5, and (D) the cell proliferation was quantitatively evaluated by CCK-8. (E) rBMSCs were directly cultured on the surface of PMMA–TBBO and PMMA–BODDB, and (F) cell morphology was captured after Phalloidin–Hoechst staining at day 5.

Since both PMMA–TBBO and PMMA–BODDB used boron-containing catalysts, bioactive boron may be released after polymerization to promote bone formation. As shown in Fig. 3E, PMMA–TBBO exhibited higher amounts of initial burst release and long-term release of boron. However, boron exhibits concentration-dependent bioactivities, and higher release rates decrease the osteogenic activity of cells.[26,27] Therefore, PMMA–BODDB, with its lower amounts of released boron, may be more suitable for osteogenesis.

Additionally, we employed UV spectroscopy to detect the release of residual monomers after PMMA polymerization (Fig. 3F and G). The characteristic peak of MMA monomers appeared at 206 nm. The residual monomer releases after soaking in PBS for 1 day and 5 days were 4.95 and 2.81 for PMMA–BODDB, respectively, which were significantly lower than the values for PMMA–BPO (17.16 and 18.30) and PMMA–TBBO (6.01 and 4.05) (Fig. 3H).

In vitro biosafety of the PMMA–BODDB bone cement

We evaluated the cell compatibility of PMMA–BODDB using two methods: extract medium culture and direct contact culture. Firstly, we prepared extracts of various PMMA by immersing these bone cement in the medium for 24 h (Fig. 4A). The BPO group exhibited sparse amounts of cell skeletons due to the high amounts of residual monomers and continuous generation of free radicals, while the cell skeletons in the TBBO and BODDB groups appeared well-defined, (Fig. 4B) exhibiting good spreading status and fewer red fluorescent signals representing dead cells (Fig. 4C). As shown in Fig. 4D, the optical density (O.D.) values of rBMSCs that grew in various extracts were on the order of BPO < TCPs < TBBO < BODDB. In other words, the extract from the BPO group inhibited cell proliferation, resulting in only 57–80% relative cell viability, while PMMA–BODDB promoted the proliferation of rBMSCs. Furthermore, we compared the cell skeletons and cell proliferation (Fig. S8, ESI†) of rBMSCs directly cultured on the surface of PMMA–TBBO and PMMA–BODDB (Fig. 4E, ESI†) and found no significant differences between the two groups (Fig. 4F).

In vitro osteoconductive capacity of the PMMA–BODDB bone cement

To investigate the osteoconductive capacity of PMMA–BODDB, we use an osteogenic induction medium to prepare osteogenic extracts. Alizarin Red staining was used to detect calcium deposition, while two protein markers (ALP, COL-I) and two genes (OPN, OCN) closely associated with BMSC osteogenic differentiation were examined (Fig. 5A). Images of the ALP staining at 7 days and the ARS staining at 14 days showed increases in ALP production and mineral deposits induced by osteogenic extracts from PMMA–BODDB as compared with the other two PMMA groups and the TCPs control group (Fig. 5B).

As for protein and gene expression, the activity of ALP protein reached the highest level on the 7th day (Fig. 5C) while COL-I synthesis gradually increased within 14 days (Fig. 5D). Similarly, the expression levels of OPN genes peaked on the 7th day, (Fig. 5E) while OCN gene expression continued to increase from 3 to 14 days (Fig. 5F). Overall, the expression of all these protein markers and genes in the BPO group was lower than in the TCP group, indicating that PMMA–BPO plays a negative role in the osteogenic differentiation of rBMSCs. However, after culturing with the osteogenic extracts of PMMA–TBBO and PMMA–BODDB, rBMSCs showed enhanced osteogenic

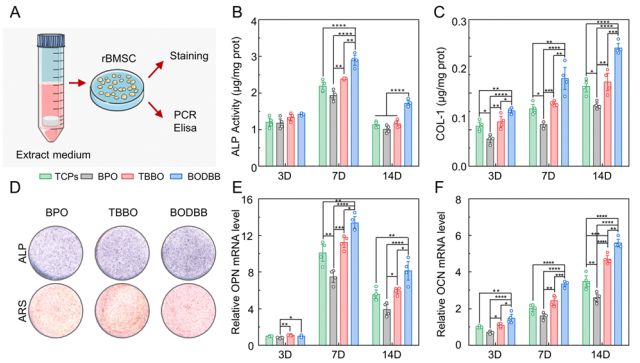

Fig. 5 (A) Schematic diagram of the osteogenic differentiation of rBMSCs cultured in various osteogenic extracts. (B) ALP activity, (D) COL-1 content, (D) ALP and ARS staining, (E) OPN gene, and (F) OCN gene expression of rBMSCs cultured in various osteogenic extracts.

differentiation, which is consistent with a previous report.[24] Importantly, PMMA–BODBB exhibited a significantly greater ability to promote rBMSC osteogenic differentiation compared to other groups. Such enhancement is likely attributed to the reduced release of free radicals and toxic monomers and moderate bioactive boron release from PMMA–BODBB catalyzed by highly purified BODBB.

Osteoconductive capacity of the PMMA–BODBB bone cement

In order to validate the osteogenic capacity of PMMA–BODBB *in vivo*, we surgically created 5 mm defects in rat calvaria[28] (Fig. 6A). The defects were filled with PMMA–BPO (Heraeus), PMMA–TBBO, and PMMA–BODBB, respectively. At each time point, the new bone formation in the defects area was firstly imaged with micro-CT as shown in Fig. 6B. Although PMMA–BPO could be visualized in CT scans due to the contained ZrO_2, the materials could be distinguished from newly formed bone according to the threshold. 4 weeks post-implantation, the blank control group exhibited almost no new bone formation, and the defect maintained its circular shape which was in accordance with previous reports.[29] The PMMA–BPO group not only showed less new bone formation at the defect site, but also experienced bone resorption in the surrounding host bone, leading to a roughened bone surface. Furthermore, there were also signs of brain damage observed in the PMMA–BPO group (Fig. S9, ESI†). This phenomenon appeared to be more severe than what was reported previously,[6] possibly due to the *in vitro* pre-solidifying process of PMMA–BPO before implantation, which avoids the intense exothermic polymerization process. In this study, however, to simulate the actual surgical procedure, we directly mixed and placed the various components of the PMMA–BPO composite at the defect site. The *in situ* polymerization process generated excessive heat and released a significant amount of residual monomers, causing thermal damage and chemical toxicity to the surrounding tissues, thus resulting in bone resorption. In contrast, both PMMA–TBBO and PMMA–BODBB showed observable new bone formation at the edges of the defect. After 8 weeks, the bone resorption in the BPO group showed some relief; however, the

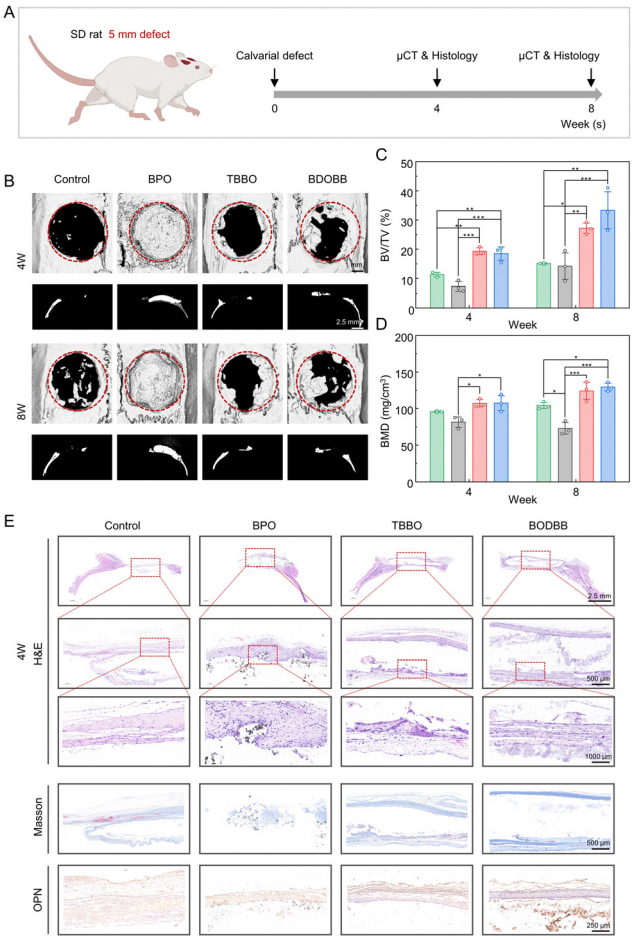

Fig. 6 The *in vivo* bone regeneration in a 5 mm rat calvarial defect model. (A) Experimental grouping and corresponding Micro-CT images, (B) BV/TV, and (C) BMD values of the bone defects 8 weeks post-operation. The diameter of red circles = 5 mm. (D) H&E staining, (E) Masson's trichrome staining, and (F) OPN immunohistochemical staining of obtained tissue section.

amount of newly formed bone was still less than that in the blank control group. The PMMA–BODBB group exhibited the highest level of new bone formation. Based on these micro-CT images, quantification including the BV/TV (new bone volume/total volume) and the BMD (bone mineral density) values were applied to reveal the quantity and the quality of the newly formed bone. Fig. 6C and D 8 weeks post-operation, the PMMA–BODBB group demonstrated the highest BV/TV (33.33%) and BMD values (129.36 mg cm^{-3}), which were 2.34 times and 1.77 times of those in the PMMA–BPO group, respectively.

Hematoxylin–eosin (H&E), Masson's trichrome staining, and OPN immunohistochemical staining were applied to further confirm the maturation of the newly formed bone[30] (Fig. 6A and Fig. S10, ESI†). The cavities observed in the stained sections represented the implanted bone cement. From 4 to 8 weeks post-operation, the defect area in the blank control group was mainly composed of fibrous tissue, exhibiting few indications of new bone formation. When the defect site was filled with PMMA–BPO, the newly formed tissue appeared

 This journal is © The Royal Society of Chemistry 2024

relatively loose and displayed the significant presence of inflammatory cells. Even with an extended repair time, the bone integration was still poor. In contrast, the defect area of the TBBO and BODBB groups showed minimal inflammatory reactions and fibrous connective tissue, with the material surface being covered by a substantial amount of collagen-rich extracellular matrix. With time, the evident formation of new bone was observed at the interface between the materials and the surrounding tissues, indicating the superior bone integration abilities of PMMA–TBBO and PMMA–BODBB. Immunohistochemical staining for OPN, a protein closely associated with osteogenesis and highly expressed in newly formed bone tissue,[31] was further performed. As shown in the figure, the expression level of OPN was significantly higher in the BODBB group compared to the blank control group and the BPO group, followed by the TBBO group. These consistent findings affirm that PMMA–BODBB exhibits superior biocompatibility and more robust bone integration capabilities in comparison to traditional PMMA–BPO and PMMA–TBBO. This makes it a promising and innovative bone cement for clinical application in the fields of orthopedics and plastic surgery.

Conclusions

In conclusion, to achieve low-temperature polymerization of PMMA bone cement with exceptional biocompatibility and osteointegration, we designed three industrial-scale synthesis methods for high-purity BODBB with excellent storage safety. Our efforts resulted in achieving a maximum purity of 97.6 ± 0.8% with a productive rate of 85.4 ± 3.7%, employing BODBB as a catalyst, we prepared PMMA bone cement (PMMA–BODBB), possessing mechanical properties comparable to PMMA–BPO and PMMA–TBBO, while exhibiting reduced release of toxic monomers, along with moderate bioactive boron release. *In vitro* studies demonstrated that PMMA–BODBB displays superior cell adhesion, proliferation, and osteogenesis. Furthermore, the promotive effect of PMMA–BODBB on bone regeneration was validated by repairing 5-mm rat calvarial defects, with the new bone volume fraction (BV/TV) and bone mineral density (BMD) reaching 33.33% and 129.36 mg cm^{-3}, respectively. This study not only presents an industrial-scale synthesis of high-purity BODBB but also introduces an innovative PMMA biomaterial system with intrinsic biocompatibility and osseointegration potential. Looking ahead, PMMA–BODBB holds promise as a fundamental material that can be synergistically integrated with various bioactive factors, thereby enhancing the functionalities and clinical applicability of PMMA-based biomaterials.

Author contributions

Zhuo Wan: conceptualization, investigation, data curation, visualization, formal analysis, writing – original draft; Yike Gao: investigation, methodology, data curation, writing – original draft; Yingbo Wang: visualization, validation, formal analysis; Xianghao Zhang: resources, funding acquisition, supervision; Xiyin Gao: software, methodology; Tuanfeng Zhou: formal analysis, writing – review & editing; Zhishan Zhang: visualization, resources, validation; Zijian Li: resources, validation; Yunfei Lin: investigation, visualization; Bing Wang: resources; Kun Chen: investigation, data curation; Yang Wang: resources, supervision; Chenggang Duan: project administration, writing – review & editing; Zuoying Yuan: conceptualization, funding acquisition, formal analysis, writing – original draft, writing – review & editing.

Data availability

The raw data required to reproduce these findings are available from the authors upon request.

Conflicts of interest

There are no conflicts to declare.

Acknowledgements

This work was financially supported by the Beijing Natural Science Foundation (No. 7244516) and the China Postdoctoral Science Foundation funded project (No. 2024M750112).

Notes and references

1 M. A. Fernandez, J. Achten, N. Parsons, X. L. Griffin, M.-E. Png, J. Gould, A. McGibbon and M. L. Costa, *N. Engl. J. Med.*, 2022, **386**, 521–530.
2 V. J. Suhardi, D. A. Bichara, S. J. J. Kwok, A. A. Freiberg, H. Rubash, H. Malchau, S. H. Yun, O. K. Muratoglu and E. Oral, *Nat. Biomed. Eng.*, 2017, **1**, 0080.
3 Z. He, Q. Zhai, M. Hu, C. Cao, J. Wang, H. Yang and B. Li, *J. Orthop. Transl.*, 2015, **3**, 1–11.
4 S. Ghosh, M. Sinha, R. Samanta, S. Sadhasivam, A. Bhattacharyya, A. Nandy, S. Saini, N. Tandon, H. Singh, S. Gupta, A. Chauhan, K. K. Aavula, S. S. Varghese, P. Shi, S. Ghosh, M. K. Garg, T. Saha, A. Padhye, S. Ghosh, H. L. Jang and S. Sengupta, *Nat. Biomed. Eng.*, 2022, **6**, 1180–1195.
5 G. Lewis, *J. Biomed. Mater. Res., Part B*, 2008, **84b**, 301–319.
6 C. Li, J. Sun, K. Shi, J. Long, L. Li, Y. Lai and L. Qin, *J. Mater. Chem. B*, 2020, **8**, 4575–4586.
7 N. J. Shah, M. N. Hyder, J. S. Moskowitz, M. A. Quadir, S. W. Morton, H. J. Seeherman, R. F. Padera, M. Spector and P. T. Hammond, *Sci. Transl. Med.*, 2013, **5**, 191ra83.
8 A. Hoess, A. López, H. Engqvist, M. K. Ott and C. Persson, *Mater. Sci. Eng., C*, 2016, **62**, 274–282.
9 E. M. Sheafi and K. E. Tanner, *J. Mech. Behav. Biomed. Mater.*, 2015, **51**, 380–387.
10 J. Schmolders, G. T. R. Hischebeth, M. J. Friedrich, T. M. Randau, M. D. Wimmer, H. Kohlhof, E. Molitor and S. Gravius, *BMC Infect. Dis.*, 2014, **14**, 144.

11 Z. Li, J. Shi, Y. Wang, Y. Li, W. Liu, R. Xu, S. Wang, L. Chen, X. Ye, C. Zhang and W. Xu, *Eng. Regen.*, 2023, **4**, 375–386.
12 M. Hossain, J. H. Jeong, T. Sultana, J. H. Kim, J. E. Moon and S. Im, *J. Biomed. Mater. Res., Part B*, 2023, **111**, 1813–1823.
13 R. Dua, Sf Li, Xy Li, Xh Bai, Yl Wang, Pf Han and Hz Li, *PLoS One*, 2024, **19**, 0299325.
14 Y. Wang, S. Shen, T. Hu, G. R. Williams, Y. Bian, B. Feng, R. Liang and X. Weng, *ACS Nano*, 2021, **15**, 9732–9745.
15 Q. C. Tan, X. S. Jiang, L. Chen, J. F. Huang, Q. X. Zhou, J. Wang, Y. Zhao, B. Zhang, Y.-N. Sun, M. Wei, X. Zhao, Z. Yang, W. Lei, Y. F. Tang and Z.-X. Wu, *Mater. Today Bio*, 2023, **18**, 100500.
16 H. Zhang, Y. Cui, X. Zhuo, J. Kim, H. Li, S. Li, H. Yang, K. Su, C. Liu, P. Tian, X. Li, L. Li, D. Wang, L. Zhao, J. Wang, X. Cui, B. Li and H. Pan, *ACS Appl. Mater. Interfaces*, 2022, **14**, 51711–51727.
17 X. Sun, X. Zhang, X. Jiao, J. Ma, X. Liu, H. Yang, K. Shen, Y. Gan, J. Wang, H. Li and W. Jin, *Bio-Des. Manuf.*, 2022, **5**, 318–332.
18 L. Chen, Y. Tang, K. Zhao, X. Zha, J. Liu, H. Bai and Z. Wu, *Colloids Surf., B*, 2019, **183**, 110448.
19 N. Tsukimura, M. Yamada, H. Aita, N. Hori, F. Yoshino, M. Chang-Il Lee, K. Kimoto, A. Jewett and T. Ogawa, *Biomaterials*, 2009, **30**, 3378–3389.
20 M. Yamada, N. Kojima, A. Paranjpe, W. Att, H. Aita, A. Jewett and T. Ogawa, *J. Dent. Res.*, 2008, **87**, 372–377.
21 N. Nakabayashi, E. Masuhara, E. Mochida and I. Ohmori, *J. Biomed. Mater. Res.*, 2004, **12**, 149–165.
22 K. Naito, *J. Oral Sci.*, 2011, **53**, 109–116.
23 K. Hamajima, R. Ozawa, J. Saruta, M. Saita, H. Kitajima, S. R. Taleghani, D. Usami, D. Goharian, M. Uno, K. Miyazawa, S. Goto, K. Tsukinoki and T. Ogawa, *Int. J. Mol. Sci.*, 2020, **21**, 4016.
24 K. Komatsu, K. Hamajima, R. Ozawa, H. Kitajima, T. Matsuura and T. Ogawa, *Cells*, 2022, **11**, 3999.
25 Y. Okamoto, K. Takahata and K. Saeki, *Chem. Lett.*, 1998, 1247–1248.
26 H. Jodati, A. Tezcaner, A. Z. Alshemary, V. Şahin and Z. Evis, *Ceram. Int.*, 2022, **48**, 22743–22758.
27 M. Gizer, S. Köse, B. Karaosmanoglu, E. Z. Taskiran, A. Berkkan, M. Timuçin, F. Korkusuz and P. Korkusuz, *Biol. Trace Elem. Res.*, 2020, **193**, 364–376.
28 Z. Wan, Z. Yuan, Y. Li, Y. Zhang, Y. Wang, Y. Yu, J. Mao, Q. Cai and X. Yang, *Adv. Funct. Mater.*, 2022, **32**, 2113280.
29 Y. Gao, Z. Yuan, X. Yuan, Z. Wan, Y. Yu, Q. Zhan, Y. Zhao, J. Han, J. Huang, C. Xiong and Q. Cai, *Bioact. Mater.*, 2022, **14**, 377–388.
30 Z. Yuan, P. Wei, Y. Huang, W. Zhang, F. Chen, X. Zhang, J. Mao, D. Chen, Q. Cai and X. Yang, *Acta Biomater.*, 2019, **85**, 294–309.
31 Z. Yuan, Z. Wan, P. Wei, X. Lu, J. Mao, Q. Cai, X. Zhang and X. Yang, *Adv. Healthcare Mater.*, 2020, **9**, e2000211.

This journal is © The Royal Society of Chemistry 2024